

<https://doi.org/10.1038/s44306-024-00023-6>

# Spintronics meets orbitronics: Emergence of orbital angular momentum in solids

Daeyeon Jo<sup>1,2,3</sup>, Dongwook Go<sup>4</sup>, Gyung-Min Choi<sup>5,6</sup> & Hyun-Woo Lee<sup>1</sup> ✉

One of the ultimate goals of spintronics is to realize an efficient electrical manipulation of spin for high-speed and low-power nanodevices. A core ingredient for achieving this goal is the relativistic interaction between the electron's orbital motion and spin, but the properties of the orbital angular momentum itself have remained largely unexplored. However, recent theories and experiments have uncovered that electrons may acquire nonvanishing orbital angular momentum when an external electric field is applied, even without the spin–orbit coupling. These findings have spurred the emergence of a burgeoning field known as orbitronics, which harnesses the orbital angular momentum to manipulate magnetic devices. In this Review, we provide an overview of the recent developments in orbitronics and discuss their implications for spintronics. We then outline future avenues of research at the intersection of spintronics and orbitronics.

Understanding and utilizing spin dynamics are primary goals of spintronics. The spin–orbit coupling (SOC)  $\sim \mathbf{S} \cdot \mathbf{L}$ , where  $\mathbf{L}$  and  $\mathbf{S}$  are the orbital angular momentum (OAM) and spin operators, respectively, is an important source of spin dynamics, and understanding its effect has been a main research theme of the spin-orbitronics field in the last decade. The SOC can induce spin splitting in noncentrosymmetric systems, and an electric field applied to such spin-split systems can generate spin density (spin Edelstein effect (SEE)<sup>1</sup>). The SOC can also induce the spin Berry curvature, and an electric field applied to systems with the spin Berry curvature generates a spin current flowing in a transverse direction to the field (spin Hall effect (SHE)) (Fig. 1a).

However, most of the previous spin-orbitronics studies dealt with the spin and orbital degrees of freedom in a biased way; Whereas the spin degree of freedom was examined in terms of both eigenstates in equilibrium and steady states in driven situations (for instance, driven by an external electric field), the orbital degree of freedom was examined only in terms of equilibrium eigenstate properties. *Nonequilibrium steady state* properties of the orbital degree of freedom rarely received attention.

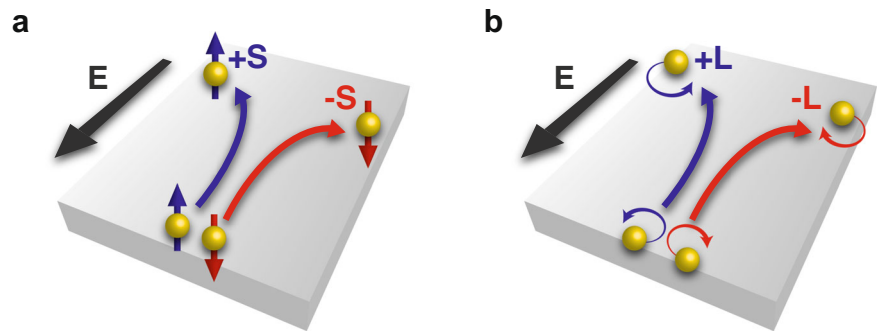
On the other hand, there was a small number of theoretical studies that examined the properties of the orbital degree of freedom in the presence of an external electric field. In particular, the calculation results published in 2008<sup>2</sup> and 2009<sup>3</sup> reported that the giant SHE of 4d and 5d transition metals is due to OAM transport generated by an electric field and concluded that the

orbital Hall effect (OHE) is the origin of the giant SHE in these materials. The OHE is the orbital counterpart of the SHE; an external electric field generates an orbital current flowing in a transverse direction to the field, as schematically depicted in Fig. 1b. To be more precise, the orbital current generated by the OHE is the OAM current, where the OAM direction of electrons determines the transverse flow direction. Thus, these results<sup>2,3</sup> contradict the common belief that the OAM is quenched in solids unless an OAM is induced by a spin through the SOC. Another notable theoretical result was published a few years earlier, which reported that the OHE occurs in hole-doped Si<sup>4</sup>, a system with an extremely weak SOC. The authors of ref. 4 anticipated that the OAM may play similar roles as the spin and coined the term orbitronics. However, this prediction and other related theoretical predictions<sup>2,3,5–10</sup> on the orbital transport did not receive much attention for a long time. One of the reasons is the widespread expectation that the OAM is quenched in solids except when it is induced by the SOC in spin-split materials (such as ferromagnets (FM)). Another important reason is the inability to probe the orbital transport experimentally.

The situation has changed in the last few years. The recent surge of interest in orbitronics is motivated by a number of recent theoretical and experimental advances. On the theory side, it was realized that the quenching of the OAM can be lifted without the SOC in various ways. In materials where the inversion symmetry is broken, the OAM expectation value of eigenstates can have nonvanishing values without being aided by

<sup>1</sup>Department of Physics, Pohang University of Science and Technology, Pohang 37673, Korea. <sup>2</sup>Department of Physics and Astronomy, Uppsala University, P.O. Box 516, SE-75120 Uppsala, Sweden. <sup>3</sup>Wallenberg Initiative Materials Science for Sustainability, Uppsala University, SE-75120 Uppsala, Sweden. <sup>4</sup>Institute of Physics, Johannes Gutenberg University Mainz, 55099 Mainz, Germany. <sup>5</sup>Department of Energy Science, Sungkyunkwan University, Suwon, Korea. <sup>6</sup>Center for Integrated Nanostructure Physics, Institute for Basic Science, Suwon, Korea. ✉e-mail: [hwl@postech.ac.kr](mailto:hwl@postech.ac.kr)

**Fig. 1** | Schematic illustration of SHE (a) and OHE (b).



SOC<sup>11–14</sup>. Such inversion-symmetry-breaking-induced OAM expectation values vary with the crystal momentum  $\mathbf{k}$  and can be nonvanishing for all crystal momentum  $\mathbf{k}$  except time-reversal-invariant-momenta such as  $\mathbf{k} = \mathbf{0}$ . Such  $\mathbf{k}$ -dependent OAM expectation values imply the orbital Rashba coupling, the orbital counterpart of the famous spin Rashba coupling. An external electric field applied to systems with the orbital Rashba coupling generates the OAM density, which is known as the orbital Edelstein effect (OEE)<sup>15–17</sup>. In materials with the inversion symmetry, the OAM expectation value may vanish for energy eigenstates in equilibrium but have nonvanishing values for steady states in the presence of an external electric field, even if the SOC is negligible<sup>18,19</sup>. Such electric-field-driven OAM implies the OHE. Both the inversion-symmetry-breaking-induced OAM in equilibrium<sup>14,20,21</sup> and the electric-field-driven OAM in nonequilibrium steady states<sup>22–28</sup> turn out to be generic in many materials.

Another group of advances occurred on the experimental side, combined with the theoretical advances on the measurable consequences of the OAM. The theoretical prediction<sup>11</sup> of the orbital Rashba effect led to the orbital-based mechanism of the spin Rashba effect. It was experimentally demonstrated that the maximal spin Rashba coupling can be realized by maximizing the orbital Rashba coupling<sup>29</sup>. It was predicted<sup>30,31</sup> that the injection of the OAM current into an FM can induce a torque (orbital torque), just as the injection of the spin current into an FM can induce torque (spin torque). This prediction was verified by numerous experiments<sup>32–36</sup>. In particular, it was demonstrated that the orbital torque may be larger than the spin torque<sup>33,34</sup>. A third type of torque was also demonstrated experimentally<sup>37,38</sup>, which combines the processes to generate the spin torque and the orbital torque. In this torque generation process, an orbital current generated in a nonmagnet (NM) is first injected into a heavy metal, where the OAM-to-spin conversion occurs through the strong SOC. The converted spin current is then injected into an FM to generate torque. We note that all three types of torque consist of the same three processes: charge-to-orbital conversion, orbital-to-spin conversion, and spin-to-magnetization transfer. Whereas the spin-to-magnetization transfer occurs in FM for all three types of torque, the locations of the charge-to-orbital conversion and the orbital-to-spin conversion differ among the torque types. For the spin torque, both conversion processes occur in NM, whereas for the orbital torque, the charge-to-orbital conversion occurs in NM and the orbital-to-spin conversion occurs in FM. For the third type of torque, on the other hand, the charge-to-orbital conversion occurs in NM and the orbital-to-spin conversion occurs in the heavy metal. Thus, all three key processes occur at different locations in the case of the third type of torque. This separation in locations provides an opportunity to separately optimize each process by adopting proper NM, heavy metals, and FM. There were also experiments to verify the orbital current in alternative ways. Considering that orbital torque detection always involves the transmission of an orbital current through an interface, which is poorly understood yet, a few groups<sup>39,40</sup> probed the orbital current within a single-layer system. In such experiments, where the orbital current transmission through interfaces is not involved at all, the existence of the orbital current is verified by optically measuring the orbital accumulation at surfaces of the system

through the magneto-optical Kerr effect. A recent experiment<sup>41</sup> on the orbital Hanle magnetoresistance, which is the orbital counterpart of the spin Hanle magnetoresistance, also verified the orbital current.

This review is organized as follows. Section “Theoretical background” provides the theoretical background for the OAM generation processes. In the section “Experimental detection of OAM current”, recent advances in the experimental detection of OHE are summarized. Finally, the section “Future directions and prospects” provides the authors’ view of the future directions of orbitronics.

## Theoretical background

### Orbital quenching and OAM generation

The orbital quenching is a consequence resulting from the crystal field. In an octahedron with the point group  $O_h$ , for example, the crystal field splits  $d$  orbital levels into  $t_{2g}$  level with  $d_{xy}$ ,  $d_{yz}$ , and  $d_{zx}$  orbitals, and  $e_g$  level with  $d_{x^2-y^2}$  and  $d_{z^2}$  orbitals. Furthermore, the difference of the amplitudes and phases among various hoppings ( $\sigma$ ,  $\pi$ ,  $\delta$ ) makes the kinetic energy anisotropic in  $\mathbf{k}$ -space. As a result, most of the bands become orbital-singlet states having real-orbital characters. That is, the Hamiltonian does not commute with the OAM operators, implying that the OAM is not a good quantum number of the system. These real-valued orbital wave functions are described by the so-called cubic harmonics, and the expectation values of the OAM operator  $\mathbf{L} = -i\hbar(\mathbf{r} \times \nabla)$  between them are identically zero. To lift this orbital quenching, the time-reversal or spatial inversion symmetry should be broken. The orbital hybridization induced by the symmetry breaking deforms the orbital wave function to have a nonvanishing OAM expectation value and have nonzero overlap with spherical harmonics, which are linear combinations of the cubic harmonics with complex coefficients, e.g.,  $|Y_2^{\pm 1}\rangle = (|d_{zx}\rangle \pm i|d_{yz}\rangle)/\sqrt{2}$ . Such a process can occur intrinsically in materials with the broken inversion or broken time-reversal symmetry. Such a process can also occur in centrosymmetric nonmagnetic systems, where the OAM is quenched in equilibrium, provided an external perturbation is applied to break one of the symmetries. For example, a considerable orbital magnetization can be induced by an external magnetic field in transition metals<sup>42</sup>, which purely originates from the coupling between the OAM and magnetic field regardless of the SOC. Below we show that large orbital generation are also feasible by an electric field that couples to the orbital degree of freedom through the crystal momentum  $\mathbf{k}$  in solids.

### Orbital Rashba effect and orbital Edelstein effect

The orbital Rashba effect, arising from the inversion symmetry breaking, manifests as a splitting of energy levels based on the OAM<sup>11,43</sup>. For a two-dimensional system with the unit normal vector  $\hat{\mathbf{z}}$ , the orbital Rashba coupling near  $\mathbf{k} = 0$  can be described by  $\mathbf{L} \cdot (\hat{\mathbf{z}} \times \mathbf{k})$ . It allows the eigenstate  $|u_{n\mathbf{k}}\rangle$  to have a  $\mathbf{k}$ -dependent OAM  $\langle \mathbf{L} \rangle_{n\mathbf{k}} \equiv \langle u_{n\mathbf{k}} | \mathbf{L} | u_{n\mathbf{k}} \rangle$  along the direction  $\hat{\mathbf{z}} \times \mathbf{k}$ . Here,  $n$  denotes a band index. Thus,  $\langle \mathbf{L} \rangle_{n\mathbf{k}}$  forms a chiral OAM texture in momentum space (Fig. 2a). The orbital Rashba coupling arises solely from the inversion symmetry breaking<sup>11–14</sup> and does not resort to relativistic corrections. This orbital Rashba coupling has been highlighted as a key

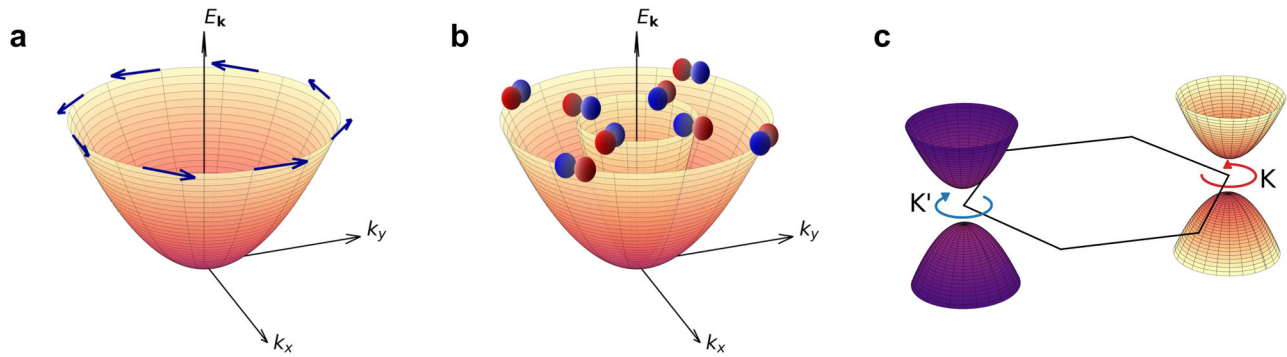


**Fig. 2 | Schematic illustrations of the band structures giving rise to nonequilibrium OAM.** **a** Rashba-type texture of the OAM in orbital Rashba systems. The navy arrows indicate the directions of the expectation values of the OAM. The electric field induces the orbital Edelstein effect. **b** Orbital texture in a

centrosymmetric *p*-orbital system. The inner and outer bands exhibit radial and tangential orbital characters, respectively. **c** Valley-dependent OAM in transition metal dichalcogenide monolayers, with positive OAM at the *K* point and negative OAM at the *K'* point. The electric field generates the OHE in (b) and (c).

element in the realization of a large Rashba spin-splitting with the assistance of the SOC, which is vital for spintronics applications<sup>21,29</sup>.

Although the orbital quenching is already lifted for each eigenstate in orbital Rashba systems, the net OAM integrated over the Fermi surface should vanish due to the constraint  $\langle \mathbf{L} \rangle_{\mathbf{n}\mathbf{k}} = -\langle \mathbf{L} \rangle_{\mathbf{n},-\mathbf{k}}$  imposed by the time-reversal symmetry. However, this cancellation disappears when an external electric field is applied, by which a dissipative charge transport breaks the time-reversal symmetry. As the electric field shifts the Fermi surface, the nonequilibrium electron populations result in a nonzero net OAM. This phenomenon amounts to the OEE<sup>14,44</sup>.

In diverse noncentrosymmetric systems, the OEE dominates over the SEE<sup>1</sup> since the former is of nonrelativistic origin, whereas the latter is of relativistic origin. Large OEE has been demonstrated in collinear antiferromagnets<sup>15</sup>, two-dimensional electron gas at SrTiO<sub>3</sub> interfaces<sup>17</sup>, surface-oxidized Cu<sup>45</sup>, and superconductors<sup>46</sup>. Furthermore, the platform for the OEE extends to a broad range of systems of chiral crystals<sup>20,47</sup>, polar metals<sup>16</sup>, and topological materials<sup>48,49</sup>.

### Orbital Hall effect

When an external electric field is applied to noncentrosymmetric systems, the momentum-space spin texture in noncentrosymmetric systems can give rise to the SHE intrinsically<sup>50</sup>. Considering the similarity between the spin texture and the OAM texture (Fig. 2a), the analogy between the spin and OAM allows one to expect that the momentum-space OAM texture can give rise to the OHE intrinsically when an external electric field is applied. In centrosymmetric systems, on the other hand, such an analogy breaks down since the spin-momentum coupling (such as spin Rashba coupling) responsible for the spin texture is forbidden in centrosymmetric systems, whereas the orbital-momentum coupling is still allowed even in centrosymmetric systems<sup>51</sup>. A few remarks are in order on this difference. To be rigorous, the spin can couple to the momentum even in centrosymmetric systems through *three-way* couplings. For instance, the hidden Rashba coupling is possible in centrosymmetric systems<sup>52</sup> and couples the *three* degrees of freedom (spin, momentum, and sublattice). However, the spin texture due to the hidden Rashba coupling is a hidden type, that is, it vanishes upon the integration over the sublattice. Thus, the hidden Rashba coupling does not generate a net spin texture nor the intrinsic spin Hall effect. For this reason, we ignore such a three-way coupling. In contrast, the two-way coupling between orbital and momentum is possible even in centrosymmetric systems. However, the resulting orbital texture differs from the OAM texture (Fig. 2a) since the OAM expectation value of the Kramers degenerate states should vanish due to the combination of the inversion symmetry and the time-reversal symmetry. It is instead the texture of the *real* orbital character, as depicted in Fig. 2b. The intrinsic OHE in centrosymmetric systems originates from the variation of the real orbital character in momentum space, termed orbital texture<sup>18</sup>. As an illustrative

model, we consider a two-dimensional *p*-orbital system<sup>51</sup> such as *p*-doped graphane<sup>10</sup> described by an effective Hamiltonian  $\mathcal{H}(\mathbf{k}) = E_{\mathbf{r}\mathbf{k}}|u_{\mathbf{r}\mathbf{k}}\rangle\langle u_{\mathbf{r}\mathbf{k}}| + E_{\mathbf{t}\mathbf{k}}|u_{\mathbf{t}\mathbf{k}}\rangle\langle u_{\mathbf{t}\mathbf{k}}|$  with eigenstates  $|u_{\mathbf{r}\mathbf{k}}\rangle = \cos \phi_{\mathbf{k}}|p_x\rangle + \sin \phi_{\mathbf{k}}|p_y\rangle$  and  $|u_{\mathbf{t}\mathbf{k}}\rangle = -\sin \phi_{\mathbf{k}}|p_x\rangle + \cos \phi_{\mathbf{k}}|p_y\rangle$ , where  $\tan \phi_{\mathbf{k}} = k_y/k_x$ . The two bands with kinetic energies  $E_{\mathbf{r}\mathbf{k}}$  and  $E_{\mathbf{t}\mathbf{k}}$  form radial and tangential orbital textures, respectively, as shown in Fig. 2b. Under an external electric field  $\mathcal{E}_x \hat{x}$ , we consider a perturbed tangential eigenstate  $|u'_{\mathbf{t}\mathbf{k}}\rangle \approx |u_{\mathbf{t}\mathbf{k}}\rangle + e\mathcal{E}_x \langle \mathcal{A}_{\mathbf{r}\mathbf{k}} |_{\hat{x}} (E_{\mathbf{r}\mathbf{k}} - E_{\mathbf{t}\mathbf{k}})^{-1} |u_{\mathbf{r}\mathbf{k}}\rangle$  up to linear order in  $\mathcal{E}_x$ , where  $e$  is the elementary charge. Here, the orbital texture results in the imaginary Berry connection  $\mathcal{A}_{\mathbf{r}\mathbf{k}} \equiv i\langle u_{\mathbf{r}\mathbf{k}} | \partial_{\mathbf{k}} u_{\mathbf{t}\mathbf{k}} \rangle = i(\mathbf{k} \times \hat{z})/k^2$ . Thus, the nonequilibrium state has nonzero  $\langle u'_{\mathbf{t}\mathbf{k}} | L_z | u'_{\mathbf{t}\mathbf{k}} \rangle$  with opposite signs for  $\pm k_y$ <sup>18</sup>. Although the net OAM is canceled out upon the integration over the occupied states, the electron motion along the *y* direction carrying  $L_z$ , characterized by the orbital current operator  $J_y^{L_z} \equiv \frac{1}{2}(v_y L_z + L_z v_y)$ , yields a nonzero net value leading to the OHE. Since the orbital texture is a general property of multi-orbital systems<sup>18,51,53</sup>, this mechanism of the OHE is ubiquitous even if the OAM is completely quenched. Numerical studies have revealed that many transition metals exhibit gigantic OHE regardless of the strength of SOC<sup>2,3,19,24</sup>.

The OHE has been theoretically studied in various systems. In noncentrosymmetric systems, there can be an additional contribution to the OHE<sup>22,23,54,55</sup>. In transition metal dichalcogenide monolayers, for example, *K* and *K'* valleys exhibit the opposite  $\langle L_z \rangle_{\mathbf{n}\mathbf{k}}$ <sup>22,54</sup>, as depicted in Fig. 2c. Additionally, the two valleys produce opposite anomalous velocities  $(e/\hbar)\mathcal{E} \times \boldsymbol{\Omega}_{\mathbf{n}\mathbf{k}}$  under the electric field  $\mathcal{E}$ , depending on the opposite Berry curvature  $\boldsymbol{\Omega}_{\mathbf{n}\mathbf{k}}$ <sup>56</sup>. This leads to the orbital Hall current even in an insulating gap<sup>54,57</sup>. Understanding a relationship between this orbital Hall insulator and topological property<sup>55,58</sup> has emerged as an important issue. In ferromagnetic materials, other types of OHE can be generated due to the SOC<sup>25</sup>. Particularly, the broken time-reversal symmetry allows the orbital current where the direction of the OAM is parallel to that of electron motion or electric field. The investigation of the OHE has been further extended by considering the OAM beyond the intra-atomic contribution. Theoretical studies<sup>26-28,59</sup> have indicated that the inter-atomic contribution to the OHE may be considerable in some systems, raising the demand for the so-called modern theory of orbital magnetization<sup>60,61</sup>.

We note that the conventional definition of the orbital current operator, a product of the velocity and OAM operators, is incomplete in predicting experimentally measurable quantities such as an orbital accumulation. This limitation arises because the OAM is not conserved in the presence of the crystal field. A similar theoretical problem with a relation between the spin current and accumulation has been discussed, which has been solved by incorporating the spin relaxation due to the SOC<sup>62</sup>. Analogously, the orbital accumulation can be estimated by considering the relaxation of the OAM due to the crystal field into the conventional orbital

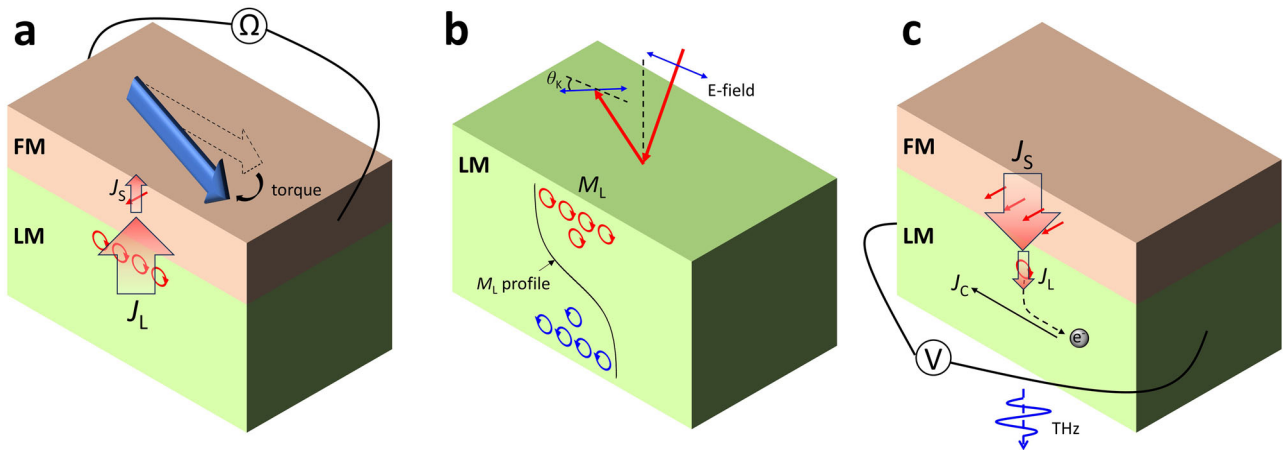


**Fig. 3 | Experimental detection of orbital currents.** **a** Detection of an orbital current via orbital torque. Orbital current ( $J_L$ ), generated in a light metal (LM), is injected into a ferromagnet (FM) and converted to spin current ( $J_S$ ) by spin-orbit coupling of FM. Then,  $J_S$  is absorbed by the magnetization of FM and induces torque. The torque-driven tilting or precession of the magnetization can be measured as magnetoresistance. **b** Detection of an orbital current via orbital accumulation. The orbital Hall effect or orbital Rashba-Edelstein effect induces orbital accumulation

( $M_L$ ) on the surfaces of the single LM layer.  $M_L$  induces Kerr rotation ( $\Delta\theta_K$ ) of the reflected light through the magneto-optical Kerr effect. The thickness profile of  $M_L$  is determined by the orbital diffusion length. **c** Detection of an orbital current via inverse effect.  $J_S$  from FM is converted to  $J_L$  by spin-orbit coupling of FM.  $J_L$  induces transverse charge current ( $J_C$ ) through the inverse orbital Hall effect or inverse orbital Rashba-Edelstein effect. The generated  $J_C$  can be measured as transverse voltage or terahertz (THz) emission<sup>81</sup>.

current<sup>39</sup>. A thorough investigation is still required to comprehend a connection between the orbital current and accumulation.

### Experimental detection of OAM current

#### Orbital torque

Spin-orbit torque measurements are widely used to investigate spin generation mechanisms in NM/FM bilayers. A spin current produced in the NM through the SHE or SEE induces spin torque on the magnetization of FM<sup>63–66</sup>. Spin-torque-driven tilting or precession of the magnetization can be measured electrically by the harmonic Hall response<sup>67</sup> or the spin-torque ferromagnetic resonance<sup>68</sup>. Similarly, an orbital current (OAM current, to be precise) produced in the NM through the OHE or OEE can induce orbital torque (Fig. 3a) on the magnetization of the FM<sup>30</sup>.

Distinguishing orbital torque from spin torque is not easy. When both spin and orbital currents are injected into the FM, torque can be expressed as

$$\text{torque} = T_S J_S + \eta_{SL} T_L J_L, \quad (1)$$

where  $J_S$  ( $J_L$ ) is the spin (orbital) current injection,  $T_S$  ( $T_L$ ) is the spin (orbital) transmission efficiency at the NM/FM interface, and  $\eta_{SL}$  is the orbital-to-spin conversion efficiency of the FM. When the SOC of the NM is weak,  $J_L$  is generally much larger than  $J_S$ <sup>24</sup>, and torque can be dominated by the orbital contribution. Thus, the observation of sizable torque in systems without any heavy elements is an indication of orbital torque. Significant torque in such heavy-element-free systems<sup>69</sup> preceded the emergence of the orbital torque concept<sup>30</sup>, and those early results were attributed to different mechanisms. After the development of the orbital torque concept, those early results were reexamined in terms of the OEE<sup>32</sup>. Later, orbital torque measurements were extended to the OHE systems with light metals of Cr, Mn, Cu, and Ti<sup>33,35,36,38</sup>.

Another important indicator of orbital torque is FM dependence. Orbital torque depends not only on the orbital generation in the NM but also on the orbital-to-spin conversion in the FM<sup>30</sup>. Experiments demonstrated that the magnitude and even the sign of orbital torque depend on the FM material and its thickness<sup>33–36,38</sup>. In addition, a large enhancement in orbital torque was achieved by inserting an additional orbital-to-spin conversion layer of Pt, Gd, or Tb between the NM and FM<sup>35,37,38</sup>.

#### Orbital accumulation

A direct measurement<sup>70</sup> of spin in an NM without an FM provides conclusive evidence for the spin generation mechanism. The SHE or SEE

induces spin accumulation on the lateral edges of semiconductor channels and on the top surfaces of heavy metals. This spin accumulation has been measured optically by the magneto-optical Kerr effect<sup>70–72</sup>. Similarly, the OHE can induce orbital accumulation on the surface of light metals (Fig. 3b) and has been detected optically in the single Ti<sup>39</sup> or Cr layer<sup>40</sup>.

Optical detection has the advantage of high orbital sensitivity. When both SHE and OHE generate spin and orbital accumulation, the Kerr rotation can be expressed as

$$\tilde{\theta}_K = O_S M_S + O_L M_L \quad (2)$$

where  $O_S$  ( $O_L$ ) is the magneto-optic constant for the unit spin (orbital) magnetization, and  $M_S$  ( $M_L$ ) is the SHE- (OHE-) induced spin (orbital) accumulation. With weak SOC of light metals, both the spin generation part ( $M_S$ ) and the spin detection part ( $O_S$ ) are strongly suppressed<sup>39,40</sup>. Accordingly, the Kerr rotation in light metals is dominated by the orbital contribution. The magnitudes of the OHE-driven Kerr rotations in Ti<sup>39</sup> and Cr<sup>40</sup> are comparable to those of the SHE-driven Kerr rotation in Pt<sup>71</sup>, demonstrating the high orbital sensitivity of the optical measurement. Recently, it was proposed that the Kerr rotation in GaAs in ref. 70 could be related to orbital accumulation rather than spin accumulation<sup>73</sup> since the SOC in GaAs is weak. With moderate SOC, the distinction between spin and orbital is challenging because both contributions can be comparable. Further research is required to separate spin and orbital accumulation in moderate SOC systems.

For a quantitative analysis of the orbital accumulation ( $M_L$ ) from the Kerr rotation,  $O_L$  should be determined. For example, the  $O_L$  value of Ti was determined from the theoretical calculation of the optical conductivity tensor and experimentally confirmed by a separate measurement of the Oersted-field-driven Kerr rotation<sup>39</sup>. In addition, the orbital diffusion length of an NM can be determined from the thickness profile of  $M_L$ <sup>39,40</sup>. Significantly different orbital lengths have been reported for Ti (74 nm)<sup>39</sup> and Cr (7 nm)<sup>40</sup>. Independent measurements of the orbital diffusivity and the orbital relaxation time would be important for a better understanding of the orbital diffusion length. A recent experiment has reported a much shorter orbital diffusion length for Ti (7.3 nm) and suggested that the length depends on the nano-structural morphology<sup>74</sup>.

## Inverse effects

As a reciprocal process of spin torque, the magnetization precession of an FM induces spin pumping, which is the generation of a spin current from a precessing FM to an NM in an FM/NM bilayer<sup>75</sup>. Spin pumping produces a transverse charge current through the inverse SHE or SEE<sup>76</sup>. When a spin current is partially converted to an orbital current within an FM by SOC, a transverse charge current in an NM could be a result of the inverse OHE or OEE (Fig. 3c). However, spin pumping is often dominant over orbital pumping; thus, making a clear distinction between spin and orbital pumping is challenging. Recently, by analyzing the angle dependence of the generated charge current as a function of the gate bias, a separation between spin pumping (combined with the inverse SEE) and orbital pumping (combined with the inverse OEE) was demonstrated in the LaAlO<sub>3</sub>/SrTiO<sub>3</sub> system<sup>77</sup>.

Ultrafast demagnetization of an FM produces an ultrafast spin current<sup>78–80</sup>. When an ultrafast spin current is injected into a heavy metal with strong SOC, the inverse SHE or SEE induces an ultrafast charge current, which can be detected as terahertz emission<sup>79</sup>. When a spin current is partially converted to an orbital current within an FM by SOC, ultrafast demagnetization can produce terahertz emission through the inverse OHE or OEE. A recent study showed that the terahertz emission in the Ni/W bilayer has the same polarity as that in the Ni/Pt bilayer<sup>81</sup>. Considering the opposite signs of the spin Hall angles of Pt and W, the observation was attributed to the inverse OEE. In addition, the terahertz emission was reported in the Co/Ti and Co/Mn bilayers, whose polarities were consistent with the inverse OHE rather than the inverse SHE<sup>82</sup>.

The combined process of the angle-dependent spin absorption at the NM/FM interface and the inverse SHE in the NM leads to spin Hall magnetoresistance in NM/FM bilayers<sup>83,84</sup>. In addition, when an external magnetic field induces spin precession through the Hanle effect, the spin Hall magnetoresistance can be achieved in a single NM layer<sup>85,86</sup>. In a weak SOC system, orbital, rather than spin, can be responsible for the magnetoresistance. Recently, orbital magnetoresistances were reported in a bilayer of permalloy/copper oxide<sup>87</sup> and a single layer of Mn<sup>41</sup>. The magnetoresistance in the permalloy/copper oxide was explained by the combination of the angle-dependent orbital absorption and inverse OEE<sup>87</sup>, and the magnetoresistance in the Mn was explained by the combination of the Hanle effect and inverse OHE<sup>41</sup>.

## Future directions and prospects

### Fully harnessing the OAM for spintronics

Despite promising theoretical results that the OAM and its current can be efficiently generated by an external electric field, there are still challenges to overcome to fully harness the OAM for spintronics. The main problem is that not all OAM contributes to the torque on the magnetization. For example, as discussed above, the OAM needs to couple to the spin to interact with the magnetization, which requires SOC. (Fig. 3a). Before and during this process, the OAM may be transferred to the lattice by exerting a mechanical torque or by generating circular phonons with finite angular momentum<sup>31</sup>. Therefore, it is necessary to find a novel mechanism by which the OAM strongly interacts with the magnetization and the loss of the OAM to the lattice system is minimized.

Achieving this goal requires a deeper understanding of the role of the crystal field potential on the induced OAM. In equilibrium, the OAM is generally quenched such that there is no transfer of angular momentum to the lattice. For non-equilibrium states, in which the OAM may be unquenched, it is not known yet how the OAM exchanges angular momentum with the lattice and what kinds of orbital dynamics are possible. Suppressing the OAM-lattice interaction may be a promising direction for fully harnessing the OAM. This is because the crystal-field potential, which does not commute with the OAM, may transfer the OAM of electrons to the lattice and exert a mechanical torque. So far, most studies have focused on materials with cubic symmetries, such as body-centered cubic and face-centered cubic crystals. It might be possible that certain classes of crystal-field splittings may suppress the OAM-lattice coupling, which, as a result,

promotes the other channel of angular momentum transfer to the spin and local moments. According to a theoretical analysis of the angular momentum transfer, angular momentum exchange between the orbital degree of freedom and the lattice is pronounced mostly at the interface under an external electric field<sup>31</sup>. Thus, engineering the interface crystal structure may open a route to enhance the efficiency of the spin-torque device using the OAM as a main source of angular momentum.

A heavy-metal insertion layer has been proposed as a strategy to enhance the orbital-to-spin conversion and demonstrated<sup>35,37</sup>. So far, only Pt<sup>35,37</sup> and a couple of 4f elements<sup>38</sup> have been shown to exhibit efficient orbital-to-spin conversion, so it is necessary to search for materials that can potentially exhibit a much higher conversion ratio from the OAM to the spin angular momentum. For example, topological insulators and semimetals with distinct band structures and spin-orbital-momentum locking may be candidate materials to be tested.

At the same time, it is highly encouraged to search for efficient orbital source materials with large OHE or OEE. So far, only transition metals have been intensively studied, but a wider range of materials, such as two-dimensional materials, topological materials, ferroelectric and magneto-electric materials, need to be investigated. In these materials, so-called non-local contribution<sup>26–28,59</sup> to the orbital angular momentum may significantly enhance the generation efficiency compared to transition metals, where the OAM is mostly centered around ionic centers.

### Orbital relaxation

Another challenge in orbitronics is to understand the relaxation mechanisms of orbitally polarized carriers. The relaxation may occur through defect scattering or even without scattering through the strong coupling of the orbital to the crystal structure and lattice vibrations. A recent theory suggested that the OAM can propagate long distances in FMs<sup>88</sup>. This feature originates from the anisotropic orbital splittings depending on the direction of the crystal momentum, where the component of the OAM parallel to the crystal momentum barely interacts with the crystal due to negligible energy splittings. Several experiments support the claim that the efficiency of the orbital torque increases with the thickness of an FM<sup>26,89,90</sup>. However, more direct testing is still necessary, for example, by tuning the crystal field splitting by external knobs that can tune the orbital splittings directly.

We also note that most of the theoretical and computational studies assumed single crystals, while the majority of experiments were performed on polycrystalline samples. Nonetheless, experiments and theories seem to agree qualitatively, and sometimes even quantitatively, in transition metal heterostructures. However, there exists also an extreme case; the prediction of a strong orbital Rashba effect has been made based on the calculation performed on a perfect alignment between Cu and O atoms<sup>45</sup>, while experimentally grown Cu oxide samples, which are naturally oxidized and thus have very complicated surface morphology and atomic arrangements<sup>91</sup>, seem to host substantial OEE, to our surprise. These empirical evidences imply that some orbitronic effects such as OHE, OEE, and orbital torque may still occur as long as local crystallinity within a single grain persists. Experimentally, this may be tested if the size of crystal grains can be systematically varied. Theoretically, it is important to clarify what types of physical mechanisms predicted for a single crystal to survive in a polycrystal and whether new effects may emerge due to scattering of orbitally polarized electrons at grain boundaries. Thus, it is highly desired to develop theories bridging the gap between single- and poly-crystalline systems.

### Phase-coherent and non-local effects

Another important aspect to be explored further is the quantum nature of orbital transport. So far, most experiments have been performed in metallic systems, where the phase coherence length is much shorter than the sample size. However, there exists a plethora of quantum transport phenomena, such as conductance quantization, Aharonov-Bohm interference, weak localization, and universal conductance fluctuation. Moreover, the manifestations of the spin degree of freedom on phase-coherent transport have also been studied, e.g., weak anti-localization. Now that the community

recently noticed the importance of orbital currents, investigation on the manifestation of the orbital degree of freedom in nanoscale and mesoscopic transport phenomena may reveal previously unnoticed insights on the quantum nature of electron transport. Manipulation of the electron's quantum state inherent in the orbital degree of freedom might offer a new direction for quantum information processing, for example, used for "flying qubits"<sup>92,93</sup>.

When the phase coherence becomes sufficiently longer than the lattice spacing, the distinction between the OAM and current becomes blurred, and we need to revisit the definition of the OAM and what we mean by orbital currents if the OAM contains both local and non-local contributions. The first step is to revisit the so-called modern theory of orbital magnetism formulated in terms of Berry phase<sup>60,61</sup>, which consistently captures all possible terms contributing to the total OAM that couples to an external magnetic field. Recent works have adopted a multi-band formulation of the modern theory and compared the results with that obtained within the atom-centered approximation for the OAM<sup>26,27</sup>. The results show that the OHEs can be substantially different depending on the definitions of the OAM. One of the main advantages of adopting the modern theory definition is that the OHE in *s* orbital systems can also be investigated, in which the OAM is due to the circulation of electrons via hoppings. For example, *s* orbital Kagome model<sup>28</sup> and the Kane–Mele model for the topological insulator<sup>94</sup> have been examined recently.

### New perspective on the orbital physics in strongly correlated materials

Contrary to spintronics, which has not paid much attention to the orbital degree of freedom for a long time, some other branches of condensed matter physics have regarded orbital physics as an important topic of research<sup>95,96</sup>. In transition metal oxides, the orbital degree of freedom plays a crucial role in inducing various competing phases in which spin, charge, and orbital orderings are often entangled. The orbital ordering has been intensively studied in various materials, including a classic *e<sub>g</sub>*-shell compound  $\text{KCuF}_3$ <sup>97</sup>, manganese compounds such as  $\text{La}_{1-x}\text{Sr}_x\text{MnO}_3$ <sup>98,99</sup>, as well as a prototypical high-temperature superconductor material  $\text{La}_{2-x}\text{Sr}_x\text{CuO}_4$ <sup>100</sup>.

In recent years, there has been noticeable progress in multi-orbital superconductivity. For example, in Fe-based unconventional superconductors, the *3d* orbitals of Fe play an important role in inducing the nematicity, spin-density-wave phase, and superconductivity<sup>101–103</sup>. Understanding the interplay among magnetism, orbital ordering, and superconductivity is one of the holy grails in the study of Fe-based superconductors<sup>104</sup>. The role of multi-orbital pairings has also been pointed out in  $\text{Sr}_2\text{RuO}_4$ <sup>105–107</sup>, a candidate material for the unconventional superconducting compounds. Meanwhile, evidence of the loop current order, which may correspond to the inter-atomic contribution of the OAM, has been found in Kagome superconductors  $\text{AV}_3\text{Sb}_5$  ( $A = \text{K}, \text{Rb}, \text{Cs}$ )<sup>108</sup>.

However, we would like to emphasize that most of the previous works on orbital physics focused mainly on the static properties in the ground state, while the excitation properties of the orbital degree of freedom in non-equilibrium remain largely unexplored, which started to receive attention only recently. Thus, we anticipate that revisiting orbital-related phenomena in oxide compounds from the orbital point of view may shed new light on the phenomena studied in the past.

### Towards orbitronics and beyond

Although orbitronics is undoubtedly helpful and promising for spintronics, it is fascinating to think about the possibility of utilizing the orbital degree of freedom itself as the main information carrier for device application. This may be developed in parallel with spintronics but could be significantly different from spintronics in that it can solve the problems that are hard to address in spintronic devices. Furthermore, one may also think of independently using orbital- and spin-polarized electrons as a *probe* to investigate orders and excitations in solids, which are expected to reveal different types of information.

We note that different versions of orbitronics have been achieved in various fields, which are all inspiring and mutually borrow ideas often. One of the most famous examples is the vortex beam in optics, which possesses a screw dislocation of phase along the propagation direction. Such light with the OAM may be utilized for imaging, spectroscopy, and communication technologies. Many methods toward this direction have been developed, and some are in a mature stage<sup>109</sup>. Analogously, magnons in a disk geometry can carry finite OAM<sup>110</sup>. Moreover, the notion of OAM and orbital transport have also been considered in some lattice models of magnons<sup>111,112</sup>. Phonons in chiral systems can carry OAM<sup>113,114</sup> and may selectively couple to magnons<sup>115</sup>. All these developments strongly suggest that orbital physics is not restricted to electrons but can be generalized to various quasi-particles and waves. Therefore, a comprehensive view of orbital physics in different research areas may bring new opportunities and give rise to interdisciplinary studies at the intersection of electronics, magnonics, phononics, and optics.

Received: 17 December 2023; Accepted: 11 April 2024;

Published online: 28 June 2024

### References

- Edelstein, V. Spin polarization of conduction electrons induced by electric current in two-dimensional asymmetric electron systems. *Solid State Commun.* **73**, 233–235 (1990).
- Tanaka, T. et al. Intrinsic spin Hall effect and orbital hall effect in *4d* and *5d* transition metals. *Phys. Rev. B* **77**, 165117 (2008).
- Kontani, H., Tanaka, T., Hirashima, D. S., Yamada, K. & Inoue, J. Giant orbital hall effect in transition metals: origin of large spin and anomalous hall effects. *Phys. Rev. Lett.* **102**, 016601 (2009).
- Bernevig, B. A., Hughes, T. L. & Zhang, S.-C. Orbitronics: the intrinsic orbital current in *p*-doped silicon. *Phys. Rev. Lett.* **95**, 066601 (2005).
- Zhang, S. & Yang, Z. Intrinsic spin and orbital angular momentum Hall effect. *Phys. Rev. Lett.* **94**, 066602 (2005).
- Guo, G. Y., Yao, Y. & Niu, Q. Ab initio calculation of the intrinsic spin Hall effect in semiconductors. *Phys. Rev. Lett.* **94**, 226601 (2005).
- Kontani, H., Naito, M., S. Hirashima, D., Yamada, K. & Inoue, J.-i Study of intrinsic spin and orbital Hall effects in *pt* based on a (*6s*, *6p*, *5d*) tight-binding model. *J. Phys. Soc. Jpn.* **76**, 103702 (2007).
- Kontani, H., Tanaka, T., Hirashima, D. S., Yamada, K. & Inoue, J. Giant intrinsic spin and orbital hall effects in  $\text{Sr}_2\text{MO}_4$  ( $m = \text{Ru}, \text{rh}, \text{mo}$ ). *Phys. Rev. Lett.* **100**, 096601 (2008).
- Tanaka, T. & Kontani, H. Intrinsic spin and orbital Hall effects in heavy-fermion systems. *Phys. Rev. B* **81**, 224401 (2010).
- Tokatly, I. V. Orbital momentum Hall effect in *p*-doped graphane. *Phys. Rev. B* **82**, 161404 (2010).
- Park, S. R., Kim, C. H., Yu, J., Han, J. H. & Kim, C. Orbital-angular-momentum based origin of Rashba-type surface band splitting. *Phys. Rev. Lett.* **107**, 156803 (2011).
- Hong, J., Rhim, J. W., Kim, C., Park, S. R. & Shim, J. H. Quantitative analysis on electric dipole energy in Rashba band splitting. *Sci. Rep.* **5**, 13488 (2015).
- Oh, S. & Choi, H. J. Orbital angular momentum analysis for giant spin splitting in solids and nanostructures. *Sci. Rep.* **7**, 2024 (2017).
- Go, D. et al. Toward surface orbitronics: giant orbital magnetism from the orbital Rashba effect at the surface of *sp*-metals. *Sci. Rep.* **7**, 46742 (2017).
- Salemi, L., Berritta, M., Nandy, A. K. & Oppeneer, P. M. Orbitally dominated Rashba–Edelstein effect in noncentrosymmetric antiferromagnets. *Nat. Commun.* **10**, 5381 (2019).
- Hara, D., Bahramy, M. S. & Murakami, S. Current-induced orbital magnetization in systems without inversion symmetry. *Phys. Rev. B* **102**, 184404 (2020).
- Johansson, A., Göbel, B., Henk, J., Bibes, M. & Mertig, I. Spin and orbital Edelstein effects in a two-dimensional electron gas: theory and application to  $\text{SrTiO}_3$  interfaces. *Phys. Rev. Res.* **3**, 013275 (2021).

18. Go, D., Jo, D., Kim, C. & Lee, H.-W. Intrinsic spin and orbital Hall effects from orbital texture. *Phys. Rev. Lett.* **121**, 086602 (2018).
19. Jo, D., Go, D. & Lee, H.-W. Gigantic intrinsic orbital Hall effects in weakly spin-orbit coupled metals. *Phys. Rev. B* **98**, 214405 (2018).
20. Yoda, T., Yokoyama, T. & Murakami, S. Orbital Edelstein effect as a condensed-matter analog of solenoids. *Nano Lett.* **18**, 916–920 (2018).
21. Bihlmayer, G., Noël, P., Vyalikh, D. V., Chulkov, E. V. & Manchon, A. Rashba-like physics in condensed matter. *Nat. Rev. Phys.* **4**, 642–659 (2022).
22. Bhowal, S. & Satpathy, S. Intrinsic orbital moment and prediction of a large orbital hall effect in two-dimensional transition metal dichalcogenides. *Phys. Rev. B* **101**, 121112 (2020).
23. Sahu, P., Bhowal, S. & Satpathy, S. Effect of the inversion symmetry breaking on the orbital hall effect: a model study. *Phys. Rev. B* **103**, 085113 (2021).
24. Salemi, L. & Oppeneer, P. M. First-principles theory of intrinsic spin and orbital Hall and Nernst effects in metallic monoatomic crystals. *Phys. Rev. Mater.* **6**, 095001 (2022).
25. Salemi, L. & Oppeneer, P. M. Theory of magnetic spin and orbital Hall and Nernst effects in bulk ferromagnets. *Phys. Rev. B* **106**, 024410 (2022).
26. Cysne, T. P., Bhowal, S., Vignale, G. & Rappoport, T. G. Orbital hall effect in bilayer transition metal dichalcogenides: from the intra-atomic approximation to the Bloch states orbital magnetic moment approach. *Phys. Rev. B* **105**, 195421 (2022).
27. Pezo, A., García Ovalle, D. & Manchon, A. Orbital hall effect in crystals: Interatomic versus intra-atomic contributions. *Phys. Rev. B* **106**, 104414 (2022).
28. Busch, O., Mertig, I. & Göbel, B. Orbital Hall effect and orbital edge states caused by *s* electrons. *Phys. Rev. Res.* **5**, 043052 (2023).
29. Sunko, V. et al. Maximal Rashba-like spin splitting via kinetic-energy-coupled inversion-symmetry breaking. *Nature* **549**, 492–496 (2017).
30. Go, D. & Lee, H.-W. Orbital torque: torque generation by orbital current injection. *Phys. Rev. Res.* **2**, 013177 (2020).
31. Go, D. et al. Theory of current-induced angular momentum transfer dynamics in spin-orbit coupled systems. *Phys. Rev. Res.* **2**, 033401 (2020).
32. Tazaki, Y. et al. Current-induced torque originating from orbital current. Preprint at arXiv:2004.09165 (2020).
33. Kim, J. et al. Nontrivial torque generation by orbital angular momentum injection in ferromagnetic-metal/Cu/Al<sub>2</sub>O<sub>3</sub> trilayers. *Phys. Rev. B* **103**, L020407 (2021).
34. Lee, D. et al. Orbital torque in magnetic bilayers. *Nat. Commun.* **12**, 6710 (2021).
35. Lee, S. et al. Efficient conversion of orbital Hall current to spin current for spin-orbit torque switching. *Commun. Phys.* **4**, 234 (2021).
36. Hayashi, H. et al. Observation of long-range orbital transport and giant orbital torque. *Commun. Phys.* **6**, 32 (2023).
37. Ding, S. et al. Harnessing orbital-to-spin conversion of interfacial orbital currents for efficient spin-orbit torques. *Phys. Rev. Lett.* **125**, 177201 (2020).
38. Sala, G. & Gambardella, P. Giant orbital Hall effect and orbital-to-spin conversion in *3d*, *5d*, and *4f* metallic heterostructures. *Phys. Rev. Res.* **4**, 033037 (2022).
39. Choi, Y.-G. et al. Observation of the orbital hall effect in a light metal Ti. *Nature* **619**, 52–56 (2023).
40. Lyalin, I., Alikhah, S., Berritta, M., Oppeneer, P. M. & Kawakami, R. K. Magneto-optical detection of the orbital Hall effect in chromium. *Phys. Rev. Lett.* **131**, 156702 (2023).
41. Sala, G., Wang, H., Legrand, W. & Gambardella, P. Orbital Hanle magnetoresistance in a *3d* transition metal. *Phys. Rev. Lett.* **131**, 156703 (2023).
42. Kubo, R. & Obata, Y. Note on the paramagnetic susceptibility and the gyromagnetic ratio in metals. *J. Phys. Soc. Jpn.* **11**, 547–550 (1956).
43. Park, J.-H., Kim, C. H., Lee, H.-W. & Han, J. H. Orbital chirality and Rashba interaction in magnetic bands. *Phys. Rev. B* **87**, 041301 (2013).
44. Yoda, T., Yokoyama, T. & Murakami, S. Current-induced orbital and spin magnetizations in crystals with helical structure. *Sci. Rep.* **5**, 12024 (2015).
45. Go, D. et al. Orbital Rashba effect in a surface-oxidized Cu film. *Phys. Rev. B* **103**, L121113 (2021).
46. Chirolli, L., Mercaldo, M. T., Guarcello, C., Giazotto, F. & Cuoco, M. Colossal orbital Edelstein effect in noncentrosymmetric superconductors. *Phys. Rev. Lett.* **128**, 217703 (2022).
47. Kim, B. et al. Optoelectronic manifestation of orbital angular momentum driven by chiral hopping in helical chains. *ACS Nano* **17**, 18873–18882 (2023).
48. Niu, C. et al. Mixed topological semimetals driven by orbital complexity in two-dimensional ferromagnets. *Nat. Commun.* **10**, 3179 (2019).
49. Osumi, K., Zhang, T. & Murakami, S. Kinetic magnetoelectric effect in topological insulators. *Commun. Phys.* **4**, 211 (2021).
50. Sinova, J. et al. Universal intrinsic spin Hall effect. *Phys. Rev. Lett.* **92**, 126603 (2004).
51. Han, S., Lee, H.-W. & Kim, K.-W. Orbital dynamics in centrosymmetric systems. *Phys. Rev. Lett.* **128**, 176601 (2022).
52. Zhang, X., Liu, Q., Luo, J.-W., Freeman, A. J. & Zunger, A. Hidden spin polarization in inversion-symmetric bulk crystals. *Nat. Phys.* **10**, 387–393 (2014).
53. Han, S., Lee, H.-W. & Kim, K.-W. Microscopic study of orbital textures. *Curr. Appl. Phys.* **50**, 13–24 (2023).
54. Canonico, L. M., Cysne, T. P., Molina-Sanchez, A., Muniz, R. B. & Rappoport, T. G. Orbital Hall insulating phase in transition metal dichalcogenide monolayers. *Phys. Rev. B* **101**, 161409 (2020).
55. Cysne, T. P. et al. Disentangling orbital and valley Hall effects in bilayers of transition metal dichalcogenides. *Phys. Rev. Lett.* **126**, 056601 (2021).
56. Xiao, D., Chang, M.-C. & Niu, Q. Berry phase effects on electronic properties. *Rev. Mod. Phys.* **82**, 1959–2007 (2010).
57. Bhowal, S. & Satpathy, S. Intrinsic orbital and spin Hall effects in monolayer transition metal dichalcogenides. *Phys. Rev. B* **102**, 035409 (2020).
58. Costa, M. et al. Connecting higher-order topology with the orbital Hall effect in monolayers of transition metal dichalcogenides. *Phys. Rev. Lett.* **130**, 116204 (2023).
59. Bhowal, S. & Vignale, G. Orbital Hall effect as an alternative to valley Hall effect in gapped graphene. *Phys. Rev. B* **103**, 195309 (2021).
60. Thonhauser, T., Ceresoli, D., Vanderbilt, D. & Resta, R. Orbital magnetization in periodic insulators. *Phys. Rev. Lett.* **95**, 137205 (2005).
61. Xiao, D., Shi, J. & Niu, Q. Berry phase correction to electron density of states in solids. *Phys. Rev. Lett.* **95**, 137204 (2005).
62. Shi, J., Zhang, P., Xiao, D. & Niu, Q. Proper definition of spin current in spin-orbit coupled systems. *Phys. Rev. Lett.* **96**, 076604 (2006).
63. Liu, L., Moriyama, T., Ralph, D. C. & Buhman, R. A. Spin-torque ferromagnetic resonance induced by the spin Hall effect. *Phys. Rev. Lett.* **106**, 036601 (2011).
64. Liu, L. et al. Spin-torque switching with the giant spin Hall effect of tantalum. *Science* **336**, 555–558 (2012).
65. Mihai Miron, I. et al. Current-driven spin torque induced by the Rashba effect in a ferromagnetic metal layer. *Nat. Mater.* **9**, 230–234 (2010).
66. Miron, I. M. et al. Perpendicular switching of a single ferromagnetic layer induced by in-plane current injection. *Nature* **476**, 189–193 (2011).

67. Pi, U. H. et al. Tilting of the spin orientation induced by Rashba effect in ferromagnetic metal layer. *Appl. Phys. Lett.* **97**, 162507 (2010).
68. Fang, D. et al. Spin-orbit-driven ferromagnetic resonance. *Nat. Nanotechnol.* **6**, 413–417 (2011).
69. An, H., Kageyama, Y., Kanno, Y., Enishi, N. & Ando, K. Spin-torque generator engineered by natural oxidation of Cu. *Nat. Commun.* **7**, 13069 (2016).
70. Kato, Y. K., Myers, R. C., Gossard, A. C. & Awschalom, D. D. Observation of the spin Hall effect in semiconductors. *Science* **306**, 1910–1913 (2004).
71. Stamm, C. et al. Magneto-optical detection of the spin Hall effect in Pt and W thin films. *Phys. Rev. Lett.* **119**, 087203 (2017).
72. Lee, W.-B. et al. Direct observation of spin accumulation and spin-orbit torque driven by Rashba-Edelstein effect in an inas quantum-well layer. *Phys. Rev. B* **104**, 184412 (2021).
73. Ovalle, D. G., Pezo, A. & Manchon, A. Orbital Kerr effect and terahertz detection via the nonlinear Hall effect. Preprint at arXiv preprint arXiv:2311.11889 (2023).
74. Idrobo, J. C. et al. Direct observation of nanometer-scale orbital angular momentum accumulation. Preprint at arXiv:2403.09269 (2024).
75. Tserkovnyak, Y., Brataas, A., Bauer, G. E. W. & Halperin, B. I. Nonlocal magnetization dynamics in ferromagnetic heterostructures. *Rev. Mod. Phys.* **77**, 1375–1421 (2005).
76. Saitoh, E., Ueda, M., Miyajima, H. & Tataru, G. Conversion of spin current into charge current at room temperature: inverse spin-Hall effect. *Appl. Phys. Lett.* **88**, 182509 (2006).
77. El Hamdi, A. et al. Observation of the orbital inverse Rashba-Edelstein effect. *Nat. Phys.* **19**, 1855–1860 (2023).
78. Malinowski, G. et al. Control of speed and efficiency of ultrafast demagnetization by direct transfer of spin angular momentum. *Nat. Phys.* **4**, 855–858 (2008).
79. Kampfrath, T. et al. Terahertz spin current pulses controlled by magnetic heterostructures. *Nat. Nanotechnol.* **8**, 256–260 (2013).
80. Choi, G.-M., Min, B.-C., Lee, K.-J. & Cahill, D. G. Spin current generated by thermally driven ultrafast demagnetization. *Nat. Commun.* **5**, 4334 (2014).
81. Seifert, T. S. et al. Time-domain observation of ballistic orbital-angular-momentum currents with giant relaxation length in tungsten. *Nat. Nanotechnol.* **18**, 1132–1138 (2023).
82. Wang, P. et al. Inverse orbital hall effect and orbitronic terahertz emission observed in the materials with weak spin-orbit coupling. *npj Quantum Mater.* **8**, 28 (2023).
83. Nakayama, H. et al. Spin Hall magnetoresistance induced by a nonequilibrium proximity effect. *Phys. Rev. Lett.* **110**, 206601 (2013).
84. Chen, Y.-T. et al. Theory of spin Hall magnetoresistance. *Phys. Rev. B* **87**, 144411 (2013).
85. Dyakonov, M. I. Magnetoresistance due to edge spin accumulation. *Phys. Rev. Lett.* **99**, 126601 (2007).
86. Vélez, S. et al. Hanle magnetoresistance in thin metal films with strong spin-orbit coupling. *Phys. Rev. Lett.* **116**, 016603 (2016).
87. Ding, S. et al. Observation of the orbital Rashba-Edelstein magnetoresistance. *Phys. Rev. Lett.* **128**, 067201 (2022).
88. Go, D. et al. Long-range orbital torque by momentum-space hotspots. *Phys. Rev. Lett.* **130**, 246701 (2023).
89. Liao, L. et al. Efficient orbital torque in polycrystalline ferromagnetic-metal/Ru/Al<sub>2</sub>O<sub>3</sub> stacks: theory and experiment. *Phys. Rev. B* **105**, 104434 (2022).
90. Bose, A. et al. Detection of long-range orbital-Hall torques. *Phys. Rev. B* **107**, 134423 (2023).
91. Gattinoni, C. & Michaelides, A. Atomistic details of oxide surfaces and surface oxidation: the example of copper and its oxides. *Surf. Sci. Rep.* **70**, 424–447 (2015).
92. DiVincenzo, D. P. The physical implementation of quantum computation. *Fortschr. Phys.* **48**, 771–783 (2000).
93. Edlbauer, H. et al. Semiconductor-based electron flying qubits: review on recent progress accelerated by numerical modelling. *EPJ Quantum Technol.* **9**, 21 (2022).
94. Pezo, A., García Ovalle, D. & Manchon, A. Orbital Hall physics in two-dimensional dirac materials. *Phys. Rev. B* **108**, 075427 (2023).
95. Tokura, Y. & Nagaosa, N. Orbital physics in transition-metal oxides. *Science* **288**, 462–468 (2000).
96. Khomskii, D. I. & Streltsov, S. V. Orbital effects in solids: basics, recent progress, and opportunities. *Chem. Rev.* **121**, 2992–3030 (2021).
97. Pavarini, E., Koch, E. & Lichtenstein, A. I. Mechanism for orbital ordering in KCuF<sub>3</sub>. *Phys. Rev. Lett.* **101**, 266405 (2008).
98. Pavarini, E. & Koch, E. Origin of Jahn-Teller distortion and orbital order in lamn<sub>3</sub>. *Phys. Rev. Lett.* **104**, 086402 (2010).
99. Mahadevan, P., Terakura, K. & Sarma, D. D. Spin, charge, and orbital ordering in La<sub>0.5</sub>Sr<sub>1.5</sub>MnO<sub>4</sub>. *Phys. Rev. Lett.* **87**, 066404 (2001).
100. Dagotto, E. Correlated electrons in high-temperature superconductors. *Rev. Mod. Phys.* **66**, 763–840 (1994).
101. Hosono, H. & Kuroki, K. Iron-based superconductors: current status of materials and pairing mechanism. *Physica C* **514**, 399–422 (2015).
102. Yi, M., Zhang, Y., Shen, Z.-X. & Lu, D. Role of the orbital degree of freedom in iron-based superconductors. *npj Quantum Mater.* **2**, 57 (2017).
103. Kontani, H., Tazai, R., Yamakawa, Y. & Onari, S. Unconventional density waves and superconductivities in Fe-based superconductors and other strongly correlated electron systems. *Adv. Phys.* **70**, 355–443 (2021).
104. Chubukov, A. V., Khodas, M. & Fernandes, R. M. Magnetism, superconductivity, and spontaneous orbital order in iron-based superconductors: which comes first and why? *Phys. Rev. X* **6**, 041045 (2016).
105. Veenstra, C. N. et al. Spin-orbital entanglement and the breakdown of singlets and triplets in SrRuO<sub>4</sub> revealed by spin- and angle-resolved photoemission spectroscopy. *Phys. Rev. Lett.* **112**, 127002 (2014).
106. Suh, H. G. et al. Stabilizing even-parity chiral superconductivity in Sr<sub>2</sub>RuO<sub>4</sub>. *Phys. Rev. Res.* **2**, 032023 (2020).
107. Ramires, A. & Sigrist, M. Identifying detrimental effects for multiorbital superconductivity: application to Sr<sub>2</sub>RuO<sub>4</sub>. *Phys. Rev. B* **94**, 104501 (2016).
108. Yin, J.-X., Lian, B. & Hasan, M. Z. Topological kagome magnets and superconductors. *Nature* **612**, 647–657 (2022).
109. Shen, Y. et al. Optical vortices 30 years on: Oam manipulation from topological charge to multiple singularities. *Light Sci. Appl.* **8**, 90 (2019).
110. Jiang, Y. et al. Twisted magnon as a magnetic tweezer. *Phys. Rev. Lett.* **124**, 217204 (2020).
111. Fishman, R. S., Gardner, J. S. & Okamoto, S. Orbital angular momentum of magnons in collinear magnets. *Phys. Rev. Lett.* **129**, 167202 (2022).
112. Go, G., An, D., Lee, H.-W. & Kim, S. K. Intrinsic magnon orbital hall effect in honeycomb antiferromagnets. Preprint at arXiv:2303.11687 (2023).
113. Ishito, K. et al. Truly chiral phonons in alpha-HgS. *Nat. Phys.* **19**, 35–39 (2023).
114. Ueda, H. et al. Chiral phonons in quartz probed by x-rays. *Nature* **618**, 946–950 (2023).
115. Liao, L. et al. Valley-selective phonon-magnon scattering in magnetoelastic superlattices. *Phys. Rev. Lett.* **131**, 176701 (2023).

## Acknowledgements

D.J. and H.-W.L. were supported by the Samsung Science and Technology Foundation (BA-1501-51). D.J. was partially supported by the Wallenberg Initiative Materials Science for Sustainability (WISE) funded by the Knut and Alice Wallenberg Foundation. G.-M.C. was supported by the National

Research Foundation of Korea (2022R1A2C1006504). D.G. was supported by Deutsche Forschungs-gemeinschaft (DFG, German Research Foundation)—TRR 173/2-268565370 (project A11), TRR 288-422213477 (project B06).

### Author contributions

H.-W.L. wrote the introduction section, D.J. the theoretical background section, G.-M.C. the experimental detection section, and D.G. the future directions section. H.-W.L. coordinated the joint writing of the manuscript.

### Competing interests

The authors declare no competing interests.

### Additional information

**Correspondence** and requests for materials should be addressed to Hyun-Woo Lee.

**Reprints and permissions information** is available at <http://www.nature.com/reprints>

**Publisher's note** Springer Nature remains neutral with regard to jurisdictional claims in published maps and institutional affiliations.

**Open Access** This article is licensed under a Creative Commons Attribution 4.0 International License, which permits use, sharing, adaptation, distribution and reproduction in any medium or format, as long as you give appropriate credit to the original author(s) and the source, provide a link to the Creative Commons licence, and indicate if changes were made. The images or other third party material in this article are included in the article's Creative Commons licence, unless indicated otherwise in a credit line to the material. If material is not included in the article's Creative Commons licence and your intended use is not permitted by statutory regulation or exceeds the permitted use, you will need to obtain permission directly from the copyright holder. To view a copy of this licence, visit <http://creativecommons.org/licenses/by/4.0/>.

© The Author(s) 2024